Chapter 5 – Acceleration of the OH + CO Reaction at Low Temperatures: Measurements of the OH (v = 0, 1) + CO Rate Constant Down to 30 K

5.1 – Abstract

The reaction between OH and CO to form H and CO_2 is important in a wide variety of systems, including atmospheric and combustion chemistry, but is complicated by a number of intermediates, including *cis*- and *trans*-HOCO and a prereactive hydrogen-bonded complex. Inspired by the high abundance of these molecules in the interstellar medium and the recent discovery of similar reactions becoming faster at low (< 100 K) temperatures, we have used the CRESU technique combined with PLP-LIF to study this rate constant down to 30 K, providing the first measurements below 80 K. Additionally, we have studied the OH (v = 1) + CO reaction, which serves as a proxy for the high-pressure termolecular rate constant of the OH (v = 0) + CO reaction, also down to 30 K. We find that the two rate constants converge at low temperatures, reaching a minimum at ~55 K, before increasing at lower temperatures. This minimum and turnaround is explained through semiclassical transition state calculations, which suggest that they are due to tunneling of the prereactive hydrogen-bonded complex to products, and competition between this and the dissociation pathway of the hydrogen-bonded complex.

5.2 – Introduction

One of the most important reactions in both atmospheric and combustion chemistry is the reaction between OH and CO

$$OH + CO \rightarrow H + CO_2 \quad \text{(R5.1)}$$

In Earth's atmosphere, this reaction is a key component in the HO_x ($HO_x = OH + HO_2$) cycle, as the atomic H produced reacts immediately with O_2 to form HO_2.

$$H + O_2 + M \rightarrow HO_2 + M \quad \text{(R5.2)}$$

The cycling of HO_x is key in understanding the oxidation processes in the atmosphere. The CO is produced from the oxidation of methane or the breakdown of larger hydrocarbons, or through anthropogenic emissions from incomplete combustion chemistry.

In combustion chemistry, on the other hand, this reaction is the final oxidation step, where the CO produced from the breakdown and oxidation of starting materials (fuels, such as propane or butane) is converted into the stable CO_2 that is ultimately emitted through the exhaust. Furthermore, it is this reaction that releases the majority of heat during combustion.[1] With the focus on decreasing CO_2 emissions into the atmosphere due to its importance in global warming and climate change, this reaction has been studied extensively at higher temperatures (up to 2500 K).

The previous measurements of this rate constant show that despite this reaction only involving four atoms, its dynamics are complex, leading to unusual temperature and pressure dependencies. At low pressures and room temperature (298 K), the rate constant remains constant, with a value on the order of 1×10^{-13} cm^3 s^{-1}, but as the density increases and approaches 1×10^{19} cm^{-3}, the rate increases to 2×10^{-13} cm^3 s^{-1}. At even higher densities, which have been measured up to 10^{22} cm^{-3} using a He buffer gas, the rate constant

increases to 1×10^{-12} cm^3 s^{-1}.[2] The high-pressure limit, however, is difficult to experimentally measure, and even at the highest pressures studied, the rate constant continues to increase. While this pressure dependence suggests a termolecular component to the reaction, the reaction's behavior suggests that it is more complicated than a third-body stabilization of the product, as in other termolecular reactions. The rate constant of ~$1\text{-}2 \times 10^{-13}$ cm^3 s^{-1} is constant over the 80 – 500 K range, before beginning to increase at higher temperatures.[2] Both the temperature and pressure dependencies of this reaction were recently evaluated and compared to results from semiclassical transition state theory by Barker et al.[3]

This unusual behavior is explained by the potential energy surface (PES) of the reaction, which shows that this reaction proceeds through multiple intermediates, as seen in Figure 5.1. The reactants initially form a weakly bound hydrogen-bonded complex (OH-CO), before passing over a small barrier to form the *trans*-HOCO intermediate, which can then proceed to isomerize through two different channels before forming the H + CO_2 products.

The unusual pressure dependence originates from competition between a termolecular reaction resulting in the stabilization of the HOCO radicals, and a chemically activated bimolecular reaction which forms H and CO_2. At low pressures, the bimolecular channel dominates, but more HOCO is stabilized as the pressure increases. Currently, the JPL Data Evaluation parameterizes this reaction by using the sum of the chemically activated bimolecular and the termolecular rate constants.[5]

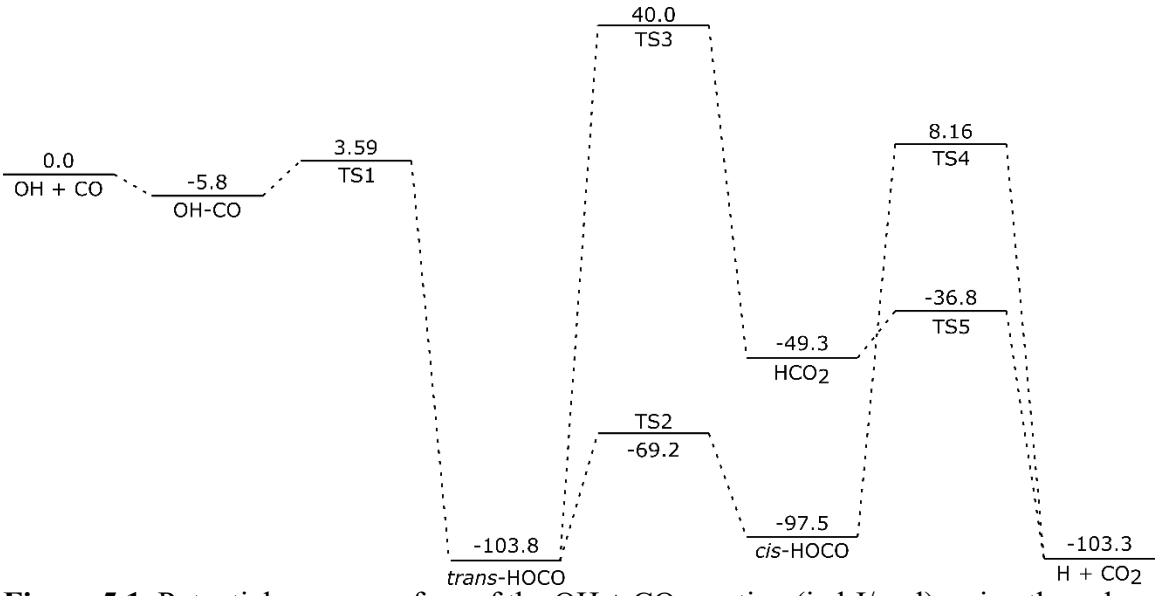

Figure 5.1: Potential energy surface of the OH + CO reaction (in kJ/mol), using the values calculated by the HEAT (High accuracy extrapolated *ab initio* thermochemistry) protocol in Nguyen et al.[4]

The HOCO intermediates were first proposed in the 1970s,[6-7] but were not directly detected from this reaction under thermal conditions until Bjork et al. in 2016, who used time resolved mid-infrared frequency comb spectroscopy to detect the *trans*-DOCO formed from OD + CO.[8] The *cis*-HOCO isomer was later directly detected using the same method in Bui et al.[9] The OH-CO hydrogen-bonded complex was suggested to play a role in the reaction from experiments down to 80 K,[10] which is to date the lowest temperature where rate constants have been measured. It has not been directly observed from this reaction, but its dynamics and stability have been studied extensively using infrared OH action spectroscopy.[11-13] These experimental values give an upper limit of 410 cm^{-1} (4.9 kJ/mol) for the dissociation energy[11], in contrast with the 5.8 kJ/mol determined from *ab initio* calculations.[4]

While experimental measurements have shown the difficulties in reaching the high-pressure limit rate constant for this reaction, it has been argued by Ian Smith and coworkers

that studying the rate constant of the reaction of vibrationally excited OH, OH (v = 1), with CO can be used as a proxy of the high pressure rate constant.[14] While the additional energy in the OH stretch is separated from the reaction coordinate and thus can not be used to proceed over TS1, if the OH (v = 1) and CO are able to overcome the barrier and result in HOCO product formation, the energy in the OH stretch will be scrambled throughout the HOCO molecules before it dissociates back to reactants, stabilizes, or proceeds to H + CO_2 products. In this way, measuring the OH (v = 1) + CO rate constant is a measurement of the rate of HOCO formation, which is equivalent to measuring the rate of the high-pressure rate constant, where only HOCO is formed, as it is the initial formation of the energetically excited HOCO that is the rate limiting step.

Thus, by monitoring OH (v = 1), the high-pressure rate constant of OH (v = 0) + CO can be determined. Previous work has demonstrated that OH (v > 0) + CO rate constants are larger than OH (v = 0), though the rate constants for OH (v = 1 – 4) + CO do not show a significant change.[15]

OH and CO are both abundant in the interstellar medium (ISM). CO is the second most common molecule throughout the ISM, with only H_2 being more abundant,[16] and is a widely used tracer for the presence of molecular clouds. In the Taurus Molecular Cloud-1 (TMC-1), CO has a fractional abundance of 10^{-4} relative to H_2,[17] while OH's fractional abundance is 10^{-7}.[18]

The possible products of this reaction are also of astrochemical interest. HOCO has not been detected in the gas or solid phases in the ISM, but it has been suggested that HOCO is a precursor that leads to the formation of glycine, the simplest amino acid, in the ISM.[19] CO_2 is ubiquitous in the ISM, with high abundances in ices but low abundances in

the gas phase.[20] However, its origins are still debated and cannot be fully explained by gas phase mechanisms alone.[20-21] The surface reaction of OH and CO on ices is believed to be important in its formation.[22]

As discussed in Chapter 1, previous studies of low temperature (< 100 K) reactions has demonstrated that some reactions reach a minimum as the temperature decreases, before increasing in rate at colder temperatures, due to the presence of prereactive hydrogen-bonded complexes. Due to the complicated PES of the OH + CO reaction suggesting that this reaction may also exhibit a rate turnaround at low temperatures, as well as their abundance in the ISM, we have studied the rate constant of this reaction down to 30 K, including measurements at different densities at 38 and 55 K. Furthermore, to determine any pressure dependencies of this reaction at low temperatures, we have also studied the reaction of OH (v = 1) + CO down to 30 K.

5.3 – Experimental Methods

Rate constants were measured using the pulsed laser photolysis-laser induced fluorescence (PLP-LIF) method in conjunction with the CRESU technique, as described previously[23-25] and in Chapter 2. Nitrogen passes through a bubbler containing 60% H_2O_2 solution (Arkema), and is mixed with a continuous flow of N_2 (99.995%, Air Liquide) and CO (99%, Air Liquide). This mix was cooled down to 30 K in an N_2 buffer gas using the CRESU technique. Briefly, a gas flow containing the reactant, CO, and radical precursor, H_2O_2, are isentropically expanded through a specially designed convergent-divergent Laval nozzle from a high-pressure reservoir into a low-pressure chamber to generate a uniform supersonic flow at the appropriate temperature with a density of $10^{16} – 10^{17}$ cm^{-3}.

Each nozzle is characterized by Pitot impact measurements prior to experiments, in order to determine the temperature, pressure and density, of the supersonic flow.

In typical CRESU experiments, concentrations of precursors and reactants are limited to < 1% of the total flow to not disrupt the flow. However, N_2 and CO are aerodynamically equivalent due to the similarities in their masses, viscosities, and heat capacity ratios, allowing us to go to much higher concentrations of CO. As seen in Figure 5.2, CRESU flows at 30 K show no difference between 100% N_2 gas flow and 50% N_2/50% CO gas flow. No signs of N_2 or CO clustering were observed in Pitot measurements down to 30 K, which would be observed as a loss of uniformity in the supersonic flow. Additional experiments used the structured LIF spectrum of the CN radical to confirm that high concentrations of CO did not affect the temperature of the flow at 38 K, using the CN generation method described in Chapter 2. The time-dependent signal of the CN radical did not change as a function of [CO], indicating that no reaction between CN and CO was occurring. The spectrum was fit with the PGOPHER program to determine the rotational temperature of CN.[26] Again, the results found no change in the temperature of the CRESU flow as the [CO] was increased.

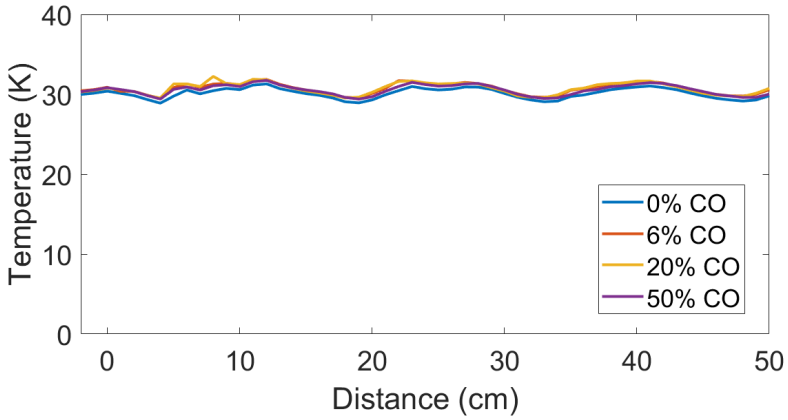

Figure 5.2: The temperatures of the 30 K nozzle, as measured by Pitot impact test measurements, at CO concentrations ranging from 0% – 50% of the total flow. No discernable change can be observed as a function of CO concentration.

OH radicals are generated by a 10 Hz excimer laser firing at 248 and 193 nm to photolyze H_2O_2, in order to form the ground and first excited vibrational states, respectively. The laser fluences at 248 and 193 nm are 31.2 and 39.5 mJ/cm^2, respectively. The second harmonic of a 10 Hz Nd:YAG laser is used to excite a dye laser containing either rhodamine 6G (for OH v = 0) or a mix of rhodamine 6G and B (for v = 1), the output of which is sent through BBO doubling crystals to produce ~1 mJ of UV light to excite the OH radicals. The (1,0) and (2,1) bands of the $A^2\Sigma^+ \leftarrow X^2\Pi$ electronic transition are used to excite the OH (v = 0) and OH (v = 1) radicals, respectively, at ~282 and ~289 nm. The resulting fluorescence is detected by a photomultiplier tube proceeded by either a 310 nm (for OH v = 0) or 320 nm (for OH v = 1) bandpass filter. The delay between the excimer and the Nd:YAG is varied from -5 – hundreds of microseconds to record the OH signal over a series of 400 evenly-spaced points, and is averaged 7-10 times to obtain the decay trace. The length of the decay is limited by the hydrodynamic time of the uniform flow of any particular nozzle. The decay is fit after 10 – 20 μs after photolysis in order to allow for rotational thermalization of the OH radical.

Kinetic measurements were taken under pseudo-first order conditions, with [CO] >> [OH]; typical CO concentrations varied from 10^{15} – 10^{16} cm^{-3}. We estimate [OH (v = 0)] to be ~2×10^{11} cm^{-3}, based on the typical H_2O_2 concentration of ~2.7×10^{13} cm^{-3} in experiments and the H_2O_2 cross sections at 248 nm (8.92×10^{-20} cm^2, OH quantum yield of 2.09 ± 0.36).[27-28] No evidence for vibrational excitation of OH produced from the 248 nm photolysis of H_2O_2 has been observed.[28-29]

The branching fraction of OH (v = 1) from the 193 nm photolysis of H_2O_2 has not been experimentally measured; Ondrey et al. and Vaghjiani et al. estimate the upper limit

to be 5 – 15% of the total OH produced.[29-30] Based on this upper limit and the 193 nm cross section of H_2O_2 (58.9×10^{-20} cm^2, OH quantum yield 1.51 ± 0.18),[27,30] we estimate the upper limit of [OH (v = 1)] to be ~9×10^{10} cm^{-3} in our experiments.

5.4 – Theoretical Methods

Theoretical calculations were conducted by our collaborator John Barker, in collaboration with John Stanton and Lam Nguyen. They have previously calculated a high quality PES of this reaction and used it to calculate rate constants over the 100 – 2000 K range[3-4] and extended this analysis to 5 K for comparison to our experimental measurements.

The *ab initio* PES of the reaction was determined with the HEAT protocol which has been shown to produce energies accurate to < 1 kJ/mol,[31-34] with the resulting energies shown in Figure 5.1. As discussed above, experimental measurements of OH-CO complex give it a dissociation energy of 410 cm^{-1} (4.9 kJ/mol),[11] in contrast with the 5.8 kJ/mol determined with the HEAT method. At the low temperatures used in this work, the rate constants from using the experimental dissociation energy and the HEAT dissociation energy differ by roughly 15%, with the rate constants using the experimental value being faster. Here we report rate constants determined using the experimental 4.9 kJ/mol for the OH-CO hydrogen-bonded complex.

After determination of the PES, semi-classical transition state theory (SC-TST) was used to calculate the low- and high-pressure limit rate constants of the reaction. SC-TST is an extension of classical TST, which calculates the number of reactants that are able to overcome the activation energy to form products, based on the partition functions and energies of the reactants and transition state. SC-TST incorporates quantum mechanical

effects, including tunneling effects, into the TST calculations, and is a computationally inexpensive method to determine rate constants theoretically.[35] Details of the HEAT and SC-TST calculations on the OH + CO reaction have been published previously.[3-4,36]

5.5 – Experimental Results

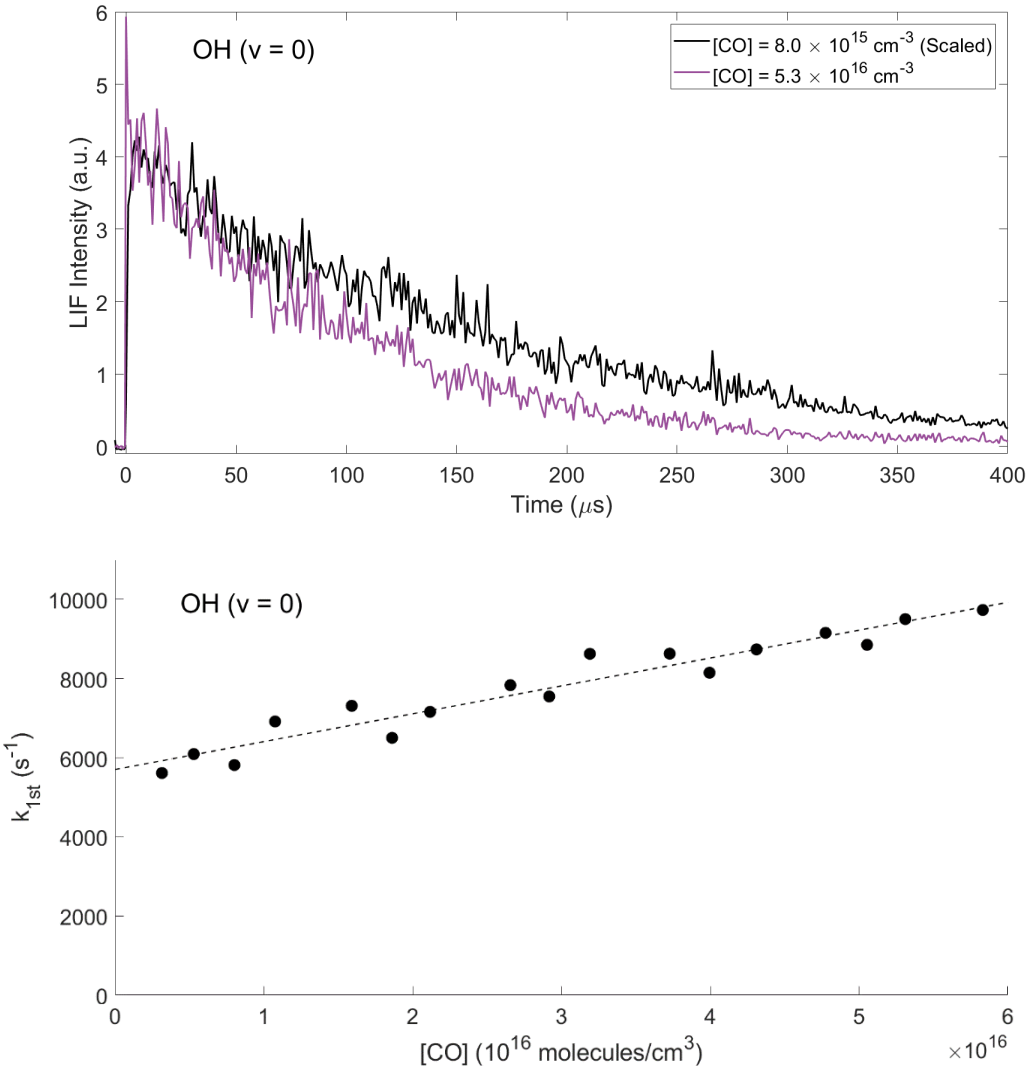

Figure 5.3: The decay of the OH (v = 0) for two different CO concentrations at 55 K (top), and the resulting second-order plot (bottom).

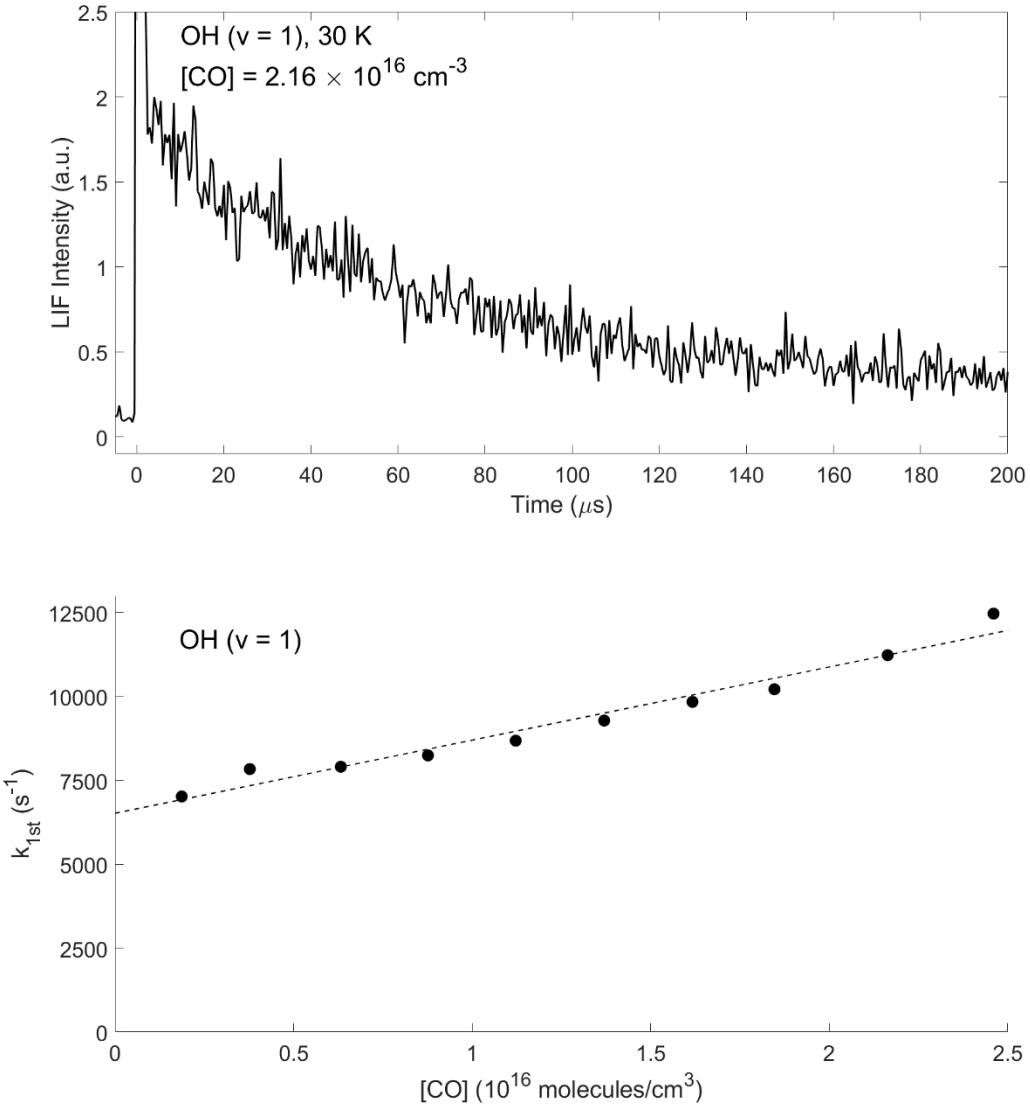

Figure 5.4: The decay of the OH (v = 1) at 30 K (top), and the resulting second-order plot (bottom).

A typical OH decay and the resulting second-order plot for OH (v = 0) and OH (v = 1) can be seen in Figures 5.3 and 5.4, respectively. The non-zero intercept on the second-order plot results from diffusion of the OH out of the region probed by LIF and from secondary chemistry resulting in OH loss. The H_2O_2 concentration and excimer laser power are kept constant for each measurement in order to prevent this secondary chemistry, such as OH + H_2O_2 and reactions of OH with other photolysis products, from interfering with

our measurements of $k_{OH + CO}$, as they will only affect the intercept on the second-order plot. We see no evidence of non-linearities in our second-order plots at high [CO], which is further evidence that CO is not clustering under our experimental conditions.

Rate constants for the OH (v = 0) + CO and OH (v = 1) + CO reactions can be seen in Tables 5.1 and 5.2, respectively, and Figure 5.5. Between 8 and 17 points at varying [CO] are taken for each measurement, in addition to points taken at the same [CO] to examine the reproducibility of the data. Measurements are taken at two densities at both 38 and 55 K to determine what effect this has on the rate constants. The v = 1 measurements display no dependence on pressure, while the results for v = 0 may display a slight dependence on pressure, but the rate coefficients fall within the experimental error. Room temperature measurements also demonstrate no pressure dependence for the v = 1 reaction; the pressure dependence of v = 0 at room temperature is well-characterized and summarized by the JPL and IUPAC data evaluations.

Table 5.1: Rate coefficients determined for the OH (v = 0) + CO reaction between 30 and 295 K, along with experimental parameters for each measurement. Uncertainties in the rate constant are the 95% confidence interval from the appropriate Student's *t* test combined in quadrature with a 10% systematic error.

Temperature (K)	Density (10^{16} cm^{-3})	[CO] range (10^{16} cm^{-3})	Number of points	$k_{OH (v = 0) + CO}$ (10^{-13} cm^3 s^{-1})
30	3.73	0.95 – 2.51	15	2.11 ± 0.37
38	3.28	0.15 – 1.97	13	0.91 ± 0.15
38	6.92	1.70 – 4.55	16	1.13 ± 0.21
55	7.06	0.32 – 5.83	17	0.70 ± 0.13
55	9.65	0.64 – 5.11	17	0.81 ± 0.19
83	4.73	0.13 – 2.22	11	1.05 ± 0.20
200	5.27	0.17 – 2.54	10	1.46 ± 0.26
295	9.50	1.44 – 7.60	11	1.44 ± 0.16

Table 5.2: Rate coefficients determined for the OH (v = 1) + CO reaction between 30 and 294 K, along with experimental parameters for each measurement. Uncertainties in the rate constant are the 95% confidence interval from the appropriate Student's *t* test combined in quadrature with a 10% systematic error. Bolded values represent the weighted average and uncertainty for temperatures with multiple measurements.

Temperature (K)	Density (10^{16} cm^{-3})	[CO] range (10^{16} cm^{-3})	Number of points	$k_{OH\ (v=1)\ +\ CO}$ (10^{-13} $cm^3\ s^{-1}$)
30	3.73	0.19 – 2.46	10	2.17 ± 0.40
38	3.28	0.15 – 1.80	12	1.30 ± 0.49
38	6.92	0.46 – 4.04	9	1.30 ± 0.45
				1.30 ± 0.11
55	7.05	0.45 – 4.28	10	1.09 ± 0.20
55	9.65	0.84 – 4.28	9	1.07 ± 0.33
				1.08 ± 0.03
83	4.72	0.22 – 1.98	9	1.93 ± 0.75
200	5.33	0.54 – 2.14	8	3.96 ± 1.20
294	4.50	0.67 – 2.01	11	7.62 ± 1.71
294	8.94	1.36 – 2.66	11	6.00 ± 1.94
294	14.50	0.26 – 2.81	13	6.37 ± 1.24
				6.63 ± 0.79

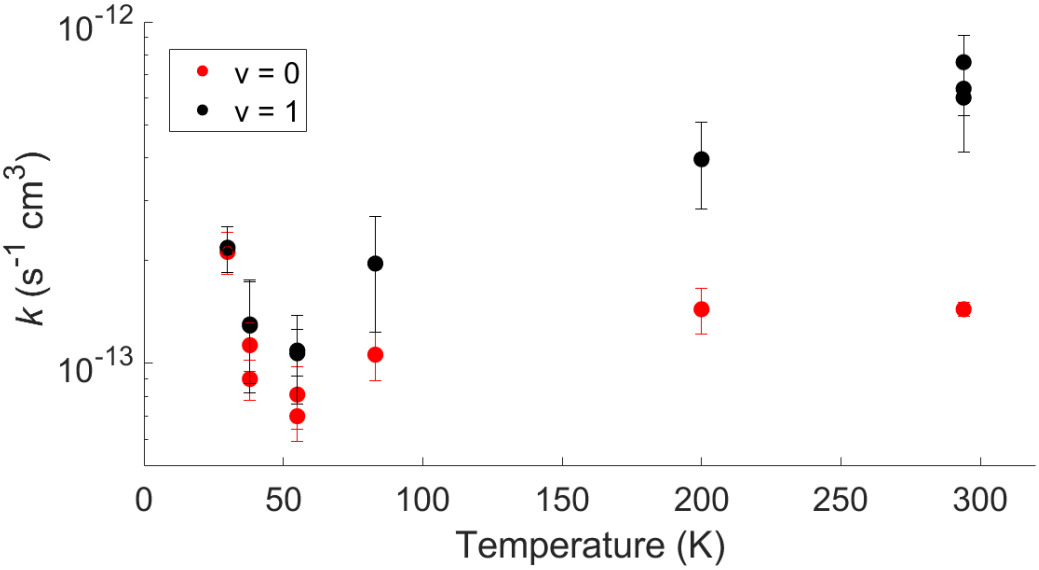

Figure 5.5: The temperature dependent rate constants of the OH (v = 0) + CO reaction (red) and the OH (v = 1) + CO reaction (black) over the 30 – 295 K range.

5.6 – Theoretical Results

The preliminary results of the SC-TST calculations by John Barker of the low-pressure limit rate constant for the OH (v = 0) + CO reaction are shown in Figure 5.6. Work on the high-pressure limit rate constants and refinement of the low-pressure limit rate constants is ongoing. Like the experimental measurements, the calculated rate constants clearly display a minimum, here located at 30 K, before increasing at lower temperatures. The calculated rate constants underestimate the experimental measurements by a factor of 2 to 5, however. It is worth noting that previous calculations using SC-TST by Barker et al. showed that the low-pressure rate constant does not change with density up to 10^{18} cm^{-3} at 100 K,[3] which suggests our results are in the low-pressure limit and the difference is not due to the densities of the nozzles.

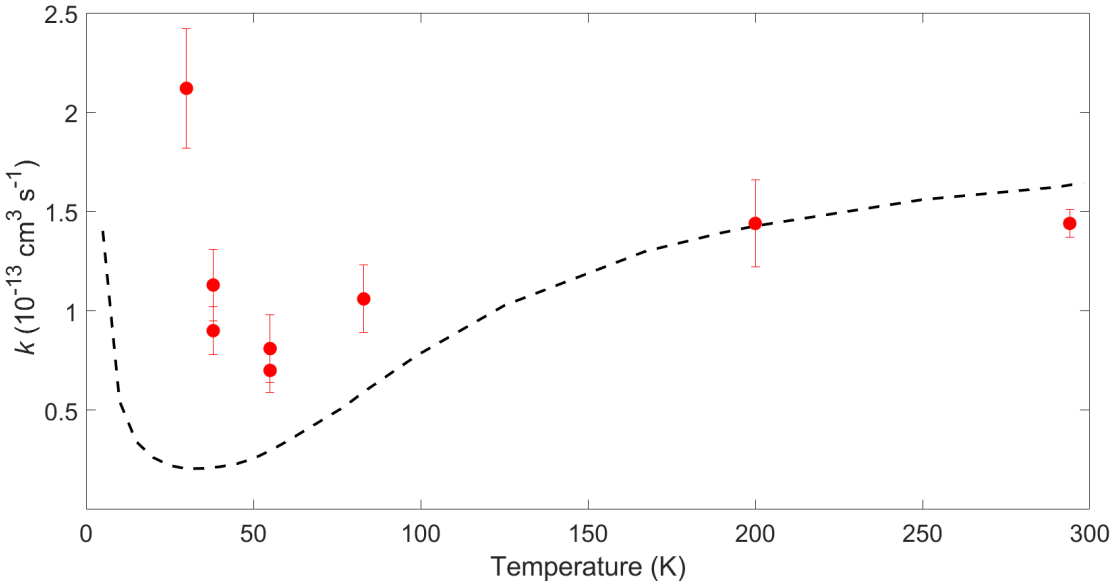

Figure 5.6: The rates of the OH (v = 0) + CO reaction measured in this work (red), as compared to the preliminary SC-TST calculations of the low-pressure limit rate constant (dashed black line).

Because the theoretical calculations are in qualitative agreement with our experimental measurements, we can use the results from the calculations to inform us of

the dynamics at play at low temperatures. This work indicates that these cold temperatures, the OH + CO proceeds through formation of the hydrogen-bonded OH-CO complex. The OH-CO complex does not become collisionally stabilized, leading it to remain thermally hot. The complex can either dissociate back to the reactants, or proceed to form HOCO via tunneling through TS1, which is 9.4 kJ/mol above the complex in energy.[4] The energy that remains in the complex allows this tunneling mechanism to proceed, where it would not be able to if it was collisionally stabilized. Like the hydrogen-bonded complex, the HOCO and HCO_2 intermediates are also not collisionally stabilized, and the products of this reaction are H and CO_2. While TS3 and TS4 are higher in energy than the reactants, it has previously been shown that H-atom tunneling plays an important role in the dissociation of the intermediates to form H and CO_2.[4]

The minimum in the rate constants and subsequent turnaround are explained through the competing fates of the hydrogen-bonded OH-CO complex, either through dissociation to reform the OH + CO reactants, or through tunneling to form the H + CO_2 products. The calculations indicate that the rates of these processes have different energy dependencies, and as the available energy changes as the temperature decreases, the fraction of the OH-CO complex that proceeds to react becomes less favorable until it reaches the minimum, after which this becomes more favorable. Further investigation into these different energy dependencies and the rate constant minimum is ongoing.

5.7 – Discussion

The rate constants for the OH (v = 0) + CO reaction at higher temperatures are in good agreement with the literature. At the 80 K measurements, Frost et al. measured the rate to be $(1.0 \pm 0.1) \times 10^{-13}$ cm^3 s^{-1},[10] which agrees with our rate of $1.05 \pm 0.20 \times 10^{-13}$ cm^3

s^{-1}. Using the values from the JPL data evaluation,[5] which give values of 1.49×10^{-13} cm^3 s^{-1} at the appropriate densities at both 200 and 295 K, agrees with our values of $(1.46 \pm 0.26) \times 10^{-13}$ cm^3 s^{-1} at 200 K and $(1.44 \pm 0.16) \times 10^{-13}$ cm^3 s^{-1} at 295 K.

The rate constant for the OH (v = 1) + CO rate constant at room temperature, however, is lower than literature values; Kohno et al. measured it to be $(10.8 \pm 0.6) \times 10^{-13}$ cm^3 s^{-1},[15] and Brunning et al. measured it to be $(10 \pm 0.2) \times 10^{-13}$ cm^3 s^{-1}.[14] The weighted average of our measurements, on the other hand, are $(6.63 \pm 0.62) \times 10^{-13}$ cm^3 s^{-1}. It is worth noting that the recent theoretical calculations from Barker et al. are unable to replicate the 10×10^{-13} cm^3 s^{-1} rate constant at the high-pressure limit at 298 K, and instead give a value of roughly 8×10^{-13} cm^3 s^{-1}.[3]

The convergence between the low- and high-pressure limit rate constants, however, is predicted by the calculations of Barker et al., who observe a similar trend at 100 K. Experimental measurements from Fulle et al. at 100 K do not show this trend,[2] but the disagreement between the high-pressure rate constants from Barker et al. and Fulle et al. has not been resolved. The work done here clearly aligns with the SC-TST results at low temperatures. Further low temperature experiments, both of the OH (v = 1) + CO rate constant and of OH (v = 0) + CO at high densities, would assist in resolving this discrepancy. The lack of pressure dependence on the rate constant suggests that the reaction is in the bimolecular regime at all pressures at cold temperatures, which is in line with the calculations indicating that H and CO_2 are the dominant products.

While other rate constants have been shown to reach a minimum before increasing in rate at lower temperatures, these reactions are all hydrogen-abstraction reactions, like OH + CH_3OH[37] and CN + C_2H_6,[38] where the hydrogen atom tunnels through the barrier to

form products. This work demonstrates that this tunneling mechanism and subsequent increase in rate constant at low temperatures can also occur for other reactions, due to the lack of collisional stabilization at low temperatures. This therefore opens the possibility for other reactions occurring through similar mechanisms.

The rate constants measured here suggest that the OH + CO reaction may play a larger role in the ISM than currently thought. Extrapolation of the our measurements to 10 K, the most used temperature in models of molecular clouds, gives a value of ~10^{-12} cm^3 s^{-1}, but current models, such as the Kinetic Database for Astrochemistry[39] (KIDA, kida.obs.u-bordeaux1.fr, accessed November 2020) give a value of 6.4 × 10^{-21} cm^3 s^{-1}, meaning the rate constant in models is off by more than 10^8 and these values should be implemented into databases. However, to confirm whether this updated rate constant actually influences chemistry in the ISM, lower temperature measurements of the reaction to better determine the rate at 10 K, and modeling of the impact of updated rate constant on the ISM are necessary.

5.8 – Conclusion

The rate constants of the reaction of the OH (v = 0, 1) + CO reactions have been determined over the 30 – 295 K range. The results show a convergence of the low-pressure rate constants, from the OH (v = 0) + CO reaction, and the high-pressure rate constants, as determined by the OH (v = 1) + CO measurements through the proxy method, which agrees with recently published SC-TST calculations. This indicates that this reaction is likely in the bimolecular regime at low temperatures and is forming H + CO_2 products. The results also show a minimum at 55 K before increasing at lower temperatures, which suggests that tunneling through the barrier may play a role in this reaction at low temperatures. This is

confirmed by preliminary SC-TST calculations performed by collaborators, which observe a similar turnaround and suggest that this is due to the competing fates of the prereactive OH-CO hydrogen-bonded complex, which can dissociate back to reactants or proceed through tunneling to result in H + CO_2 formation.

5.9 – References

1. Miller, J. A.; Kee, R. J.; Westbrook, C. K., Chemical-Kinetics and Combustion Modeling. *Annu Rev Phys Chem* **1990**, *41*, 345-387.

2. Fulle, D.; Hamann, H. F.; Hippler, H.; Troe, J., High Pressure Range of Addition Reactions of HO - 2. Temperature and Pressure Dependence of the Reaction HO + CO ↔ HOCO → H+CO_2. *J Chem Phys* **1996**, *105*, 983-1000.

3. Barker, J. R.; Stanton, J. F.; Nguyen, T. L., Semiclassical Transition State Theory/Master Equation Kinetics of HO + CO: Performance Evaluation. *Int J Chem Kinet* **2020**.

4. Nguyen, T. L.; Xue, B. C.; Weston, R. E.; Barker, J. R.; Stanton, J. F., Reaction of HO with CO: Tunneling Is Indeed Important. *J Phys Chem Lett* **2012**, *3*, 1549-1553.

5. Burkholder, J. B., et al., "Chemical Kinetics and Photochemical Data for Use in Atmospheric Studies, Evaluation No. 19" Jpl Publications 19-5, Jet Propulsion Laboratory, Pasadena, 2019 http://jpldataeval.jpl.nasa.gov Publications, J., Ed. 2019.

6. Smith, I. W. M.; Zellner, R., Rate Measurements of Reactions of OH by Resonance-Absorption - 2. Reactions of OH with CO, C_2H_4 and C_2H_2. *J Chem Soc Farad T 2* **1973**, *69*, 1617-&.

7. Smith, I. W. M., Mechanism of OH + CO Reaction and Stability of HOCO Radical. *Chem Phys Lett* **1977**, *49*, 112-115.

8. Bjork, B. J., et al., Direct Frequency Comb Measurement of OD + CO → DOCO Kinetics. *Science* **2016**, *354*, 444-448.

9. Bui, T. Q.; Bjork, B. J.; Changala, P. B.; Nguyen, T. L.; Stanton, J. F.; Okumura, M.; Ye, J., Direct Measurements of DOCO Isomers in the Kinetics of OD. *Sci Adv* **2018**, *4*.

10. Frost, M. J.; Sharkey, P.; Smith, I. W. M., Reaction between OH (OD) Radicals and CO at Temperatures Down to 80 K - Experiment and Theory. *J Phys Chem* **1993**, *97*, 12254-12259.

11. Pond, B. V.; Lester, M. I., Decay Dynamics of the Vibrationally Activated OH-CO Reactant Complex. *J Chem Phys* **2003**, *118*, 2223-2234.

12. Lester, M. I.; Pond, B. V.; Marshall, M. D.; Anderson, D. T.; Harding, L. B.; Wagner, A. F., Mapping the OH+CO → HOCO Reaction Pathway through IR Spectroscopy of the OH-CO Reactant Complex. *Faraday Discuss* **2001**, *118*, 373-385.

13. Lester, M. I.; Pond, B. V.; Anderson, D. T.; Harding, L. B.; Wagner, A. F., Exploring the OH + CO Reaction Coordinate Via Infrared Spectroscopy of the OH-CO Reactant Complex. *J Chem Phys* **2000**, *113*, 9889-9892.

14. Brunning, J.; Derbyshire, D. W.; Smith, I. W. M.; Williams, M. D., Kinetics of OH (v = 0, 1) and OD (v = 0, 1) with CO and the Mechanism of the OH + CO Reaction. *J Chem Soc Farad T 2* **1988**, *84*, 105-119.

15. Kohno, N.; Izumi, M.; Kohguchi, H.; Yamasaki, K., Acceleration of the Reaction OH + CO → H + CO_2 by Vibrational Excitation of OH. *J Phys Chem A* **2011**, *115*, 4867-4873.

16. Burgh, E. B.; France, K.; McCandliss, S. R., Direct Measurement of the Ratio of Carbon Monoxide to Molecular Hydrogen in the Diffuse Interstellar Medium. *Astrophys J* **2007**, *658*, 446-454.

17. Fuente, A., et al., Gas Phase Elemental Abundances in Molecular Clouds (GEMS) I. The Prototypical Dark Cloud TMC 1. *Astron Astrophys* **2019**, *624*.

18. Harju, J.; Winnberg, A.; Wouterloot, J. G. A., The Distribution of OH in Taurus Molecular Cloud-1. *Astron Astrophys* **2000**, *353*, 1065-1073.

19. Eckhardt, A. K.; Bergantini, A.; Singh, S. K.; Schreiner, P. R.; Kaiser, R. I., Formation of Glyoxylic Acid in Interstellar Ices: A Key Entry Point for Prebiotic Chemistry. *Angew Chem Int Edit* **2019**, *58*, 5663-5667.

20. Hasegawa, T. I.; Herbst, E.; Leung, C. M., Models of Gas-Grain Chemistry in Dense Interstellar Clouds with Complex Organic-Molecules. *Astrophys J Suppl S* **1992**, *82*, 167-195.

21. Minissale, M.; Congiu, E.; Manico, G.; Pirronello, V.; Dulieu, F., CO_2 Formation on Interstellar Dust Grains: A Detailed Study of the Barrier of the CO Plus O Channel. *Astron Astrophys* **2013**, *559*.

22. Watanabe, N.; Mouri, O.; Nagaoka, A.; Chigai, T.; Kouchi, A.; Pirronello, V., Laboratory Simulation of Competition between Hydrogenation and Photolysis in the Chemical Evolution of H_2O-CO Ice Mixtures. *Astrophys J* **2007**, *668*, 1001-1011.

23. Cooke, I. R.; Sims, I. R., Experimental Studies of Gas-Phase Reactivity in Relation to Complex Organic Molecules in Star-Forming Regions. *ACS Earth Space Chem* **2019**, *3*, 1109-1134.

24. James, P. L.; Sims, I. R.; Smith, I. W. M.; Alexander, M. H.; Yang, M. B., A Combined Experimental and Theoretical Study of Rotational Energy Transfer in Collisions between NO($X\,^2\Pi_{1/2}$, v = 3, *J*) and He, Ar and N_2 at Temperatures Down to 7 K. *J Chem Phys* **1998**, *109*, 3882-3897.

25. Sims, I. R.; Queffelec, J. L.; Defrance, A.; Rebrionrowe, C.; Travers, D.; Bocherel, P.; Rowe, B. R.; Smith, I. W. M., Ultralow Temperature Kinetics of Neutral-Neutral Reactions - the Technique and Results for the Reactions CN+O_2 Down to 13 K and CN+NH_3 Down to 25 K. *J Chem Phys* **1994**, *100*, 4229-4241.

26. Western, C. M., PGOPHER: A Program for Simulating Rotational, Vibrational and Electronic Spectra. *J Quant Spectrosc Ra* **2017**, *186*, 221-242.

27. Nicovich, J. M.; Wine, P. H., Temperature-Dependent Absorption Cross-Sections for Hydrogen-Peroxide Vapor. *J Geophys Res-Atmos* **1988**, *93*, 2417-2421.

28. Vaghjiani, G. L.; Ravishankara, A. R., Photodissociation of H_2O_2 and CH_3OOH at 248 nm and 298 K - Quantum Yields for OH, O(^{3}P) and H(^{2}S). *J Chem Phys* **1990**, *92*, 996-1003.

29. Ondrey, G.; Vanveen, N.; Bersohn, R., The State Distribution of OH Radicals Photodissociated from H_2O_2 at 193 and 248 nm. *J Chem Phys* **1983**, *78*, 3732-3737.

30. Vaghjiani, G. L.; Turnipseed, A. A.; Warren, R. F.; Ravishankara, A. R., Photodissociation of H_2O_2 at 193 and 222 nm - Products and Quantum Yields. *J Chem Phys* **1992**, *96*, 5878-5886.

31. Tajti, A.; Szalay, P. G.; Csaszar, A. G.; Kallay, M.; Gauss, J.; Valeev, E. F.; Flowers, B. A.; Vazquez, J.; Stanton, J. F., Heat: High Accuracy Extrapolated Ab Initio Thermochemistry. *J Chem Phys* **2004**, *121*, 11599-11613.

32. Bomble, Y. J.; Vazquez, J.; Kallay, M.; Michauk, C.; Szalay, P. G.; Csaszar, A. G.; Gauss, J.; Stanton, J. F., High-Accuracy Extrapolated Ab Initio Thermochemistry. II. Minor Improvements to the Protocol and a Vital Simplification. *J Chem Phys* **2006**, *125*.

33. Harding, M. E.; Vazquez, J.; Ruscic, B.; Wilson, A. K.; Gauss, J.; Stanton, J. F., High-Accuracy Extrapolated Ab Initio Thermochemistry. III. Additional Improvements and Overview. *J Chem Phys* **2008**, *128*.

34. Thorpe, J. H.; Lopez, C. A.; Nguyen, T. L.; Baraban, J. H.; Bross, D. H.; Ruscic, B.; Stanton, J. F., High-Accuracy Extrapolated Ab Initio Thermochemistry. IV. A Modified Recipe for Computational Efficiency. *J Chem Phys* **2019**, *150*.

35. Shang, X.; Burd, T. A. H.; Clary, D. C., New Developments in Semiclassical Transition-State Theory. *J Phys Chem A* **2019**, *123*, 4639-4657.

36. Weston, R. E.; Nguyen, T. L.; Stanton, J. F.; Barker, J. R., HO+CO Reaction Rates and H/D Kinetic Isotope Effects: Master Equation Models with Ab Initio SCTST Rate Constants. *J Phys Chem A* **2013**, *117*, 821-835.

37. Shannon, R. J.; Blitz, M. A.; Goddard, A.; Heard, D. E., Accelerated Chemistry in the Reaction between the Hydroxyl Radical and Methanol at Interstellar Temperatures Facilitated by Tunnelling. *Nat Chem* **2013**, *5*, 745-749.

38. Sims, I. R.; Queffelec, J. L.; Travers, D.; Rowe, B. R.; Herbert, L. B.; Karthauser, J.; Smith, I. W. M., Rate Constants for the Reactions of CN with Hydrocarbons at Low and Ultra-Low Temperatures. *Chem Phys Lett* **1993**, *211*, 461-468.

39. Wakelam, V., et al., A Kinetic Database for Astrochemistry (KIDA). *Astrophys J Suppl S* **2012**, *199*.